

Discovery of BKT correlations in the quantum kagome compound $\text{Cs}_2\text{Cu}_3\text{SnF}_{12}$

M. S. Grbić^{1,*}, I. Jakovac¹, I. Kupčić¹, H. Tanaka^{2,†} and M. Horvatić³

¹*Department of Physics, Faculty of Science, University of Zagreb, Bijenička cesta 32, 10000 Zagreb, Croatia*

²*Department of Physics, Institute of Science Tokyo, Meguro-ku, Tokyo 152-8551, Japan*

³*Laboratoire National des Champs Magnétiques Intenses, LNCMI-CNRS (UPR3228), EMFL, Université Grenoble Alpes, Université Toulouse, INSA-T, 38042 Grenoble Cedex 9, France*

(Dated: March 25, 2026)

We investigate the microscopic properties of the kagome compound $\text{Cs}_2\text{Cu}_3\text{SnF}_{12}$ using $^{63,65}\text{Cu}$ nuclear quadrupolar resonance (NQR). Analysis of the local hyperfine fields below the Néel temperature $T_N = 20$ K indicates a spin structure consistent with $P2_1/n$ symmetry of negative vector chirality. Measurements of the spin-lattice relaxation rate T_1^{-1} reveal signatures of a gapless ground state and two-dimensional Berezinskii–Kosterlitz–Thouless (BKT)–type correlations above T_N , extending over a broad temperature range of approximately 130 K in zero magnetic field. Within the same temperature range, the observed increase in the NQR linewidth is consistent with short-range chiral order recently identified by neutron scattering. Our results establish $\text{Cs}_2\text{Cu}_3\text{SnF}_{12}$ as a unique quantum kagome system exhibiting BKT behavior.

Frustrated quantum magnets, such as the spin $S = 1/2$ triangular-lattice and the kagome-lattice Heisenberg antiferromagnets, have been extensively studied because a large degeneracy of their ground state and low-dimensional enhancement of quantum fluctuations allow exotic phenomena to emerge. However, these same features make it challenging to experimentally determine the exact nature of the ground state [1], particularly if single crystals are unavailable. Despite these difficulties, significant progress has been achieved, and various quantum spin liquids, chiral orders and fractionalized excitations have been reported [2]. Surprisingly, notwithstanding the large body of work on two-dimensional (2D) systems, only a single report to date has identified 2D XY correlations of Berezinskii-Kosterlitz-Thouless (BKT) type in a frustrated lattice [3]. One strategy of studying frustrated systems is to lift the ground-state degeneracy by controlled tuning - e.g. with chemical pressure [4–6] or external strain [7] - thereby stabilizing a particular phase, that can be studied in detail.

In the family of compounds $\text{A}_2\text{Cu}_3\text{SnF}_{12}$ ($\text{A} = \text{Rb}, \text{Cs}$) [8, 9], $S = 1/2$ is borne by the copper Cu^{2+} ion enclosed in an F_6 octahedron, and the exchange interactions, mediated by the Cu-F-Cu bonds, form a kagome lattice. Cs and Rb lie outside the kagome plane and control the coupling between the layers. The two limiting cases, $\text{Rb}_2\text{Cu}_3\text{SnF}_{12}$ (RCSF) and $\text{Cs}_2\text{Cu}_3\text{SnF}_{12}$ (CCSF), show drastically different ground states. RCSF hosts a valence bond solid (VBS) singlet ground state with a particular “pinwheel” pattern [10, 11] formed by 4 different Heisenberg couplings - $J_1 = 234$ K, $J_2 = 0.95J_1$, $J_3 = 0.85J_1$, and $J_4 = 0.55J_1$. The large Dzyaloshinskii-Moriya (DM) interaction $d_i \approx 0.18J_i$ ($i = 1-4$) on each bond defines the dispersion of the energy excitations and keeps the spin polarization within the kagome plane. CCSF is closer to the isotropic kagome [12] with $J_1 = 154$ K, $J_2 = J_1$, $J_3 = 0.84J_1$, $J_4 = 0.7J_1$, where frustration is higher. Although the interlayer coupling is weak ($J'/J_1 \leq 10^{-3}$),

a larger DM interaction of opposite sign, $d_i \approx -0.29J_i$, is believed to push the system [8, 13, 14] to order below $T_N \approx 20$ K. In both systems, a perfect kagome lattice at room temperature on cooling goes through a structural transition that results with heterogeneous J values. In CCSF, a neutron scattering (NS) study [15] has shown that the rhombohedral crystal structure ($\text{R}\bar{3}\text{m}$) reduces to the monoclinic one ($P2_1/n$) below $T_t = 186$ K. The same work found that magnetic structure corresponds to the $P2_1'/n'$ symmetry with positive chirality (i.e., all-in-all-out structure). Ground state excitations were shown to display a spinon continuum [16, 17] with negative renormalization [12, 18], indicative of strong quantum effects driven by frustration and low S value. Availability of large single crystals and unconventional physics makes CCSF a model for distorted-kagome system, for both experimental and theoretical studies.

In this Letter we report on the discovery of 2D XY correlations of the Berezinskii-Kosterlitz-Thouless (BKT) type in the $S = 1/2$ kagome compound CCSF, persisting in a broad temperature range. Its appearance is accompanied by 2D short-range order, connected to a chiral state recently observed by NS. We use $^{63,65}\text{Cu}$ nuclear quadrupolar resonance (NQR) as a local experimental probe. In addition, by analyzing zero-field nuclear magnetic resonance (zf-NMR) spectra, we revise the exact spin structure of the long-range order. These results provide a very stringent framework for a theoretical description of the ground state realized in CCSF, and of 2D XY correlations in kagome compounds in general.

We first present the NQR spectral data. When a copper nucleus (spin $I = 3/2$) is at a locally non-cubic site, it shows two NQR lines for each non-equivalent position at zero magnetic field. These correspond to the two isotopes: ^{63}Cu (^{65}Cu) with gyromagnetic constants $^{63}\gamma = 11.285$ MHz/T ($^{65}\gamma = 12.089$ MHz/T), abundances of 69% (31%), respectively, and a ratio of quadrupolar moments $^{63}Q/^{65}Q = 1.0806$. The NQR fre-

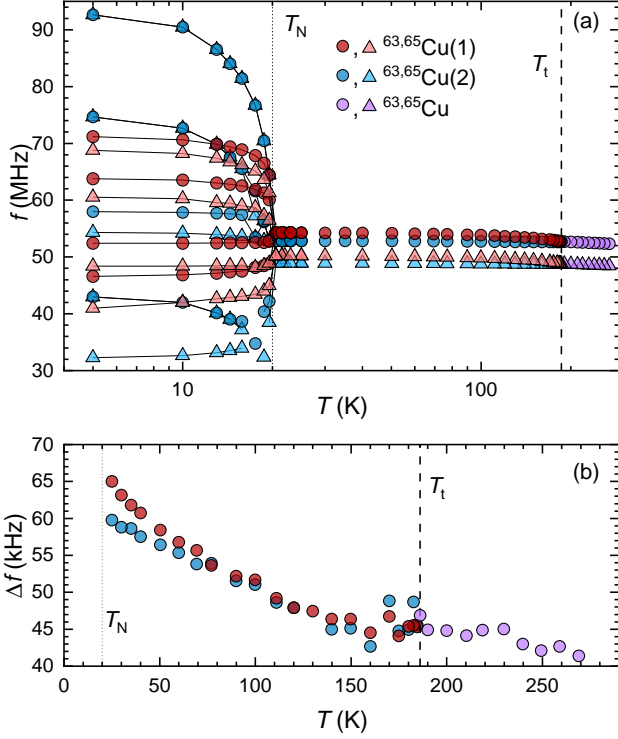


FIG. 1. (a) NQR line is split below the structural transition temperature $T_t = 186$ K. Below $T_N = 20$ K magnetic order onsets and the spectrum is further split. Circles and triangles mark the signals of $^{63,65}\text{Cu}$ isotopes. Purple marks the signal of a single crystallographic site above T_t , while red and blue mark the signals of Cu(1) and Cu(2) sites, respectively. Lines are guides for the eyes. (b) T -dependence of NQR linewidths of Cu(1,2) sites show an increase below ~ 150 K. Note that temperature scales in (a) and (b) are different.

quency is defined by the nuclear quadrupolar Hamiltonian:

$$\mathcal{H}_Q = \frac{h\nu_Q}{6} \left[3I_z^2 - I^2 + \frac{\eta_Q(I_+^2 + I_-^2)}{2} \right], \quad (1)$$

where $\nu_Q = \frac{3eQ}{2I(2I-1)}V_{zz}$, V_{zz} is the principal value of the local electric field gradient (EFG) tensor, e is the elementary charge, I_z and I_{\pm} are the standard z projection and raising (lowering) operators of the nuclear spin, and $\eta_Q = (V_{yy} - V_{xx})/V_{zz}$ is the EFG asymmetry parameter. At 290 K there is one line per isotope (Figs. 1(a) and S1) with a Lorentzian shape, with the frequency corresponding to $\nu_{\text{NQR}} = \nu_Q \sqrt{1 + \eta^2/3}$. Typical FWHM linewidth of $\Delta f \approx 43$ kHz shows the high quality of single crystals (Fig. 1(b)). As the system is cooled across the structural transition at $T_t = 186$ K, NQR signal of a single Cu site splits into two: Cu(1) and Cu(2) (Figs. 1(a) and S1). At low temperatures, CuF_6 octahedra of Cu(1,2) sites are tilted by $\alpha_{1,2} = 17.8^\circ(16^\circ)$, respectively. The angles $\alpha_{1,2}$ are defined by the average planes passing through the four nearest-neighbor F^- ions that surround

Cu, with respect to the kagome plane. These determine the orientation of the $d_{x^2-y^2}$ orbital and the orientation of the principal axes $\mathbf{e}_{\text{EFG}}(1, 2)$ corresponding to the principal value V_{zz} . NQR signal is assigned to a specific Cu site by comparing the signal intensities, which equal the structural occupancy of Cu sites in the unit cell $N[\text{Cu}(1)] : N[\text{Cu}(2)]$. The intensity ratio of 1 : 2 (Fig. S1) is consistent with the expected one from the crystal structure of Ref. [15]. As the system is cooled below ≈ 150 K, the linewidth Δf of both sites starts to increase (Fig. 1(b)), reaching 60 – 65 kHz just above T_N . This increase exactly coincides with the recently found onset of chiral state in CCSF [17], indicating that the $\Delta f(T)$ depicts the formation of short-range magnetic order, expected to emerge [19, 20] below $T \sim J$ (in our case J_1). A different chiral short-range 2D order has previously been observed in a classical kagome system [21]. When CCSF is cooled below T_N , the Néel phase onsets, and a Zeeman term $H_M = -\gamma\hbar\mathbf{B}_h\mathbf{I}$ is then added to the nuclear Hamiltonian, where \mathbf{B}_h is the local hyperfine field. The shape of the spectrum, i.e. eigenvalues of the total Hamiltonian $H = H_M + H_Q$, is defined by the field size $B_h = |\mathbf{B}_h|$, the angles (ϑ, φ) of \mathbf{B}_h with respect to \mathbf{e}_{EFG} , and the values of ν_Q and η_Q . To determine B_h , each zF-NMR signal needs to be matched to a specific Cu site. Fortunately, the five mentioned parameters are reduced to two (B_h and ϑ) as NQR frequency ν_{NQR} is measured and $\eta_Q \approx 0$ is determined in a separate experiment (Fig. S3). An additional point-charge calculation (see Supplemental Material) confirmed that $\eta_Q \approx 0$ and that the angle between \mathbf{e}_{EFG} and the kagome plane is within 2° of $\alpha_{1,2}$. Since $\eta_Q \approx 0$, the EFG tensor is axial and φ becomes irrelevant for our calculation. The main difficulty in the spectral analysis then lies in the assignment of different lines in the NMR spectrum. The correct assignment was recognized by a successful fit of exactly diagonalized Hamiltonian H to the complete spectra of both isotopes taken at different temperatures, leading to the fit parameters $B_h(i)$ and $\vartheta(i)$, where $i = 1, 2$ denotes the Cu sites. In Fig. 2(b) (and Fig. S4) we show the two sets of B_h that account for the entire spectra. Surprisingly, the B_h values are drastically different, with $B_h(1) \approx 0.5B_h(2)$. Since the NS determined [15] that $|\mathbf{m}(1)| \approx |\mathbf{m}(2)|$, these B_h values can only be explained by the magnetic moments with a distinct orientation with respect to the hyperfine coupling tensor \mathbf{A} . Magnitude of B_h is set by $\mathbf{B}_h = \mathbf{A} \cdot \mathbf{m}$, where the typical values of the \mathbf{A} for the Cu nucleus in CuF_6 [11, 22] equal $A_{\parallel} \approx -18 \text{ T}/\mu_B$ with a large anisotropy $A_{\parallel}/A_{\perp} \sim 10$. Here, “ \parallel ” denotes the principal axis of the \mathbf{A} tensor, typically parallel to \mathbf{e}_{EFG} . Therefore, $|B_h(1)| \approx 1 \text{ T}$ is realized if the moment $\mathbf{m}(1)$ is oriented close to A_{\perp} . To generate $B_h(2) \approx 2B_h(1)$, $\mathbf{m}(2)$ must form a much larger angle δ_A with respect to A_{\perp} , than $\mathbf{m}(1)$. The **all-in-all-out** spin structure that best fits the NS data is not consistent with these observations. However, it is important to note that the

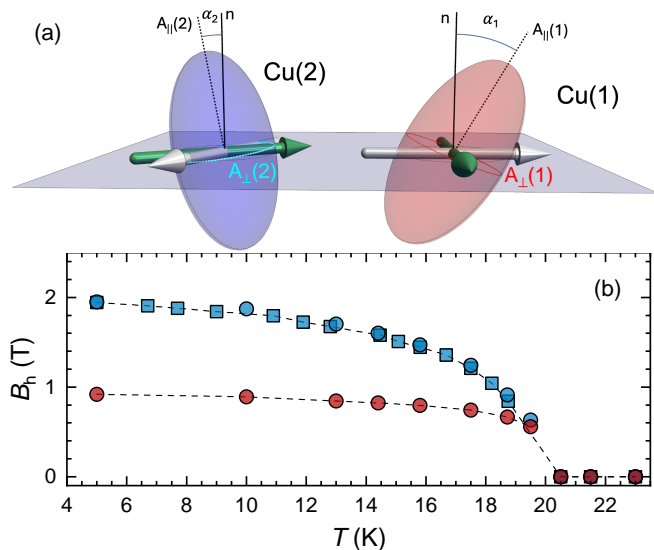


FIG. 2. (a) Depiction of the hyperfine coupling (EFG) tensor tilting for angles $\alpha_{1,2}$ with respect to the kagome plane for Cu(1) and Cu(2) sites in red and blue, respectively. Tilting angles are emphasized for clarity. Principal axes A_{\parallel} (\mathbf{e}_{EFG}) are marked with dashed black lines, kagome plane normal \mathbf{n} with full lines, A_{\perp} component in cyan and red dashed circles. 3D arrows show the spin orientation on the Cu(1,2) sites determined by Ref. [15] (gray) and this work (green). See also Fig. S5. (b) Fitting of spectra below T_N of Fig. 1(a) results with local magnetic fields on Cu(1) (red circles) and Cu(2) (blue circles). Blue squares are additional points for Cu(2) obtained by measuring only the highest-frequency line and fixing the fitting parameters obtained from the spectra.

TABLE I. Angles $\delta_A(1,2)$ between the magnetic moment $\mathbf{m}(1,2)$ and A_{\perp} component of the Cu(1,2) sites, for different spin structures proposed by neutron scattering [15]. Only structure No. 4 explains the zf-NMR data of this study.

No.	Magnetic structure (vector chirality)	angle δ_A for site	
		Cu(1)	Cu(2)
1	$P2'_1/n'(+)$	16°	16°
2	$P2'_1/n'(-)$	16°	7.8°
3	$P2_1/n(+)$	6.8°	0.1°
4	$P2_1/n(-)$	6.8°	13.9°

weak magnetic scattering intensity prevented NS to exclude any of the remaining three spin arrangements altogether. Therefore, the current data provide the complementary information required to identify the correct structure. To this end, we calculate the angles $\delta_A(1,2)$ of the symmetry-allowed spin structures found by NS for Cu(1,2) sites and show them in Table I. Only for the spin structure No. 4, having $P2_1/n$ symmetry and a negative vector chirality (-), we find that $\delta_A(2) > \delta_A(1)$ and present values that are consistent with the observed B_h values. Interestingly, this structure is a predicted [23] ground state for an isotropic kagome lattice with $d_z < 0$ (as is the case for CCSF).

To study the spin dynamics, we have measured the spin-spin (T_2^{-1}) and spin-lattice (T_1^{-1}) relaxation rates. T_2 was determined by measuring the spin echo decay using a standard Hahn sequence ($\pi/2-\tau-\pi$) and fitting the data to $M(t) = M_0 e^{-t/T_2}$. $T_2^{-1}(T)$ dependence, shown in Fig. 3(a), indicate the increase of local field fluctuations, from 270 K to low temperatures. As we approach T_N , below $\sim 25 - 30$ K, critical fluctuations of the 3D order start to build up and T_2^{-1} of both sites diverge, reaching a maximum value at T_N . At lower temperatures the fluctuations are strongly reduced and T_2 becomes longer – saturating below 5 K to a value of $25 \mu\text{s}$ for Cu(2) site. One can see that below 120-150 K ($\approx J_1$) the two Cu sites present different $T_2^{-1}(T)$ behavior, indicating that some other fluctuation mechanism sets in. To further elucidate its origin, we focus on the T_1 data presented in Fig. 3(b). T_1 time is a sensitive probe of intrinsic low-energy fluctuations of the system and is connected to the transverse spin correlation length ξ as $1/T_1 \propto \xi^{z-\eta}$, where z and η are the dynamic and static critical exponents [24]. By comparing T_1 data to ξ of different systems we can identify the nature of underlying excitations. We have measured $T_1^{-1}(T)$ in detail on the Cu(2) site, and at several temperatures on Cu(1) site to verify it shows the same behavior. Relaxation curves were measured using a saturation-pulse sequence and fitted to the expression for $I = 3/2$: $M(t) = M_0(1 - e^{-(3t/T_1)^\beta})$ where β is the stretch exponent. All the curves showed a single-component ($\beta \approx 1$) relaxation down to T_N . Generally, in antiferromagnetic insulators it is expected [25] that T_1^{-1} is temperature independent in the paramagnetic state. However, in CCSF, $T_1^{-1}(T)$ dependence shows a clear quasi-linear background already below 300 K. To verify its origin, we have measured T_1^{-1} up to 675 K (Fig. S6) and find that $T_1^{-1}(T)$ develops also a $\propto T^2$ dependence above 400 K. From this we conclude that the background is due to a two-phonon absorption processes [26] with a linear tail at low temperatures. We find the same background in the “pinwheel” VBS compound RCSF [(Fig. 3(b)) which has akin crystal structure – as expected for the phononic origin. In CCSF, T_1^{-1} rapidly decreases below T_N as the magnetic order develops; first with $T_1^{-1} \propto T^6$, and below 9 K as $\propto T^3$. The former behavior is quite common in the AF ordered states [27] and corresponds to a higher-order relaxation process [28], while the later behavior probably indicates some saturation effect, as in Ref. [29]. Both of these trends are power-laws, and show a vanishing energy scale (consistent with a small energy gap) at low temperatures. This is in-line with the NS observation of quantum spin liquid fluctuations in the ordered state [16]. Above T_N , we observe a large divergence, where T_1^{-1} is increased by more than an order of magnitude. In contrast, there is only a small increase from the structural transition at T_t . The enhanced T_1^{-1} , showing a build-up of spin fluctuations, can be traced quite high in temperature – all the way

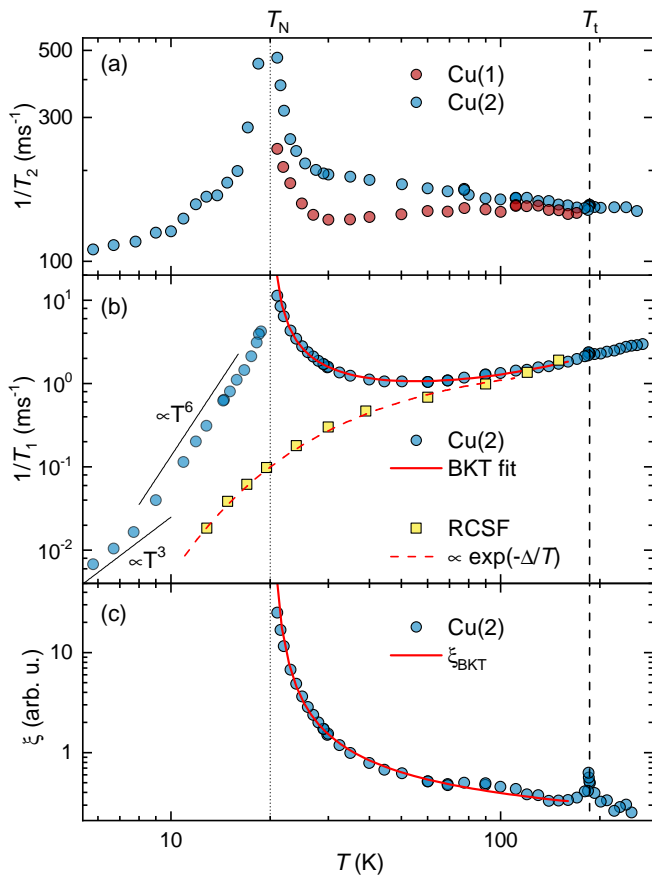


FIG. 3. (a) T_2^{-1} temperature dependence of both Cu sites. Below $T_N = 20$ K only the Cu(2) site was measured because of lower intensity of the Cu(1) site. Vertical dotted (dashed) line marks the magnetic (structural) transition temperature T_N (T_t). (b) T_1^{-1} temperature dependence of Cu(2) site. Only a small increase is seen at T_t . Below 150 K T_1^{-1} starts to monotonously increase down to T_N . Full red line is a fit $T_1^{-1} \propto \xi_{\text{BKT}}(T)^{z-\eta} + a_1T + a_2T^2$ (see main text). Below T_N , T_1^{-1} drops first rapidly ($\propto T^6$) and below 9 K $\propto T^3$ indicating a gapless ground state. For comparison, we also show relaxation of Cu in RCSF which has a singlet ground state and shows no BKT divergence (yellow squares), but a gapped relaxation $T_1^{-1} \propto \exp(-\Delta/T)$ (red dashed line). (c) $\xi_{\text{BKT}}(T)$ calculated from (b). Full red line is the fit to $\xi_0 \exp(0.5\pi/\sqrt{T/T_{\text{BKT}} - 1})$.

up to 150 K ($\approx 7T_N$). The magnitude and extent of this enhancement reveals a strong 2D character of the spin dynamics, as 3D critical excitations are typically confined within $\lesssim 10\%$ above T_N . This argument is supported by the fact that in NQR, T_2^{-1} (T_1^{-1}) probe the spin dynamics parallel (perpendicular) to \mathbf{e}_{EFG} , respectively. 3D critical fluctuations should then emerge in T_2^{-1} close to T_N , while 2D fluctuations (almost) perpendicular to \mathbf{e}_{EFG} are visible dominantly in T_1^{-1} . And indeed this is the case. We treat $T_1^{-1}(T)$ using several models (Fig. S6): 3D and 2D Heisenberg antiferromagnet, and 2D BKT correlation length of an easy-plane antiferromagnet $\xi_{\text{BKT}}(T) =$

$\xi_0 \exp(0.5\pi/\sqrt{T/T_{\text{BKT}} - 1})$. The phononic background is accounted for using a second-order polynomial in T without a constant term. We find that the fit using 2D BKT *exactly* accounts for the observed increase, with $\xi_0 = 0.186(4)$ and $T_{\text{BKT}} = 19.31(5)$ K. The T_{BKT} temperature that is very close to T_N shows that the system is strongly 2D, with the interlayer coupling [30, 31] of $J'/J_{\text{avg.}} \approx 10^{-4}$. $\xi_{\text{BKT}}(T)$ has a characteristic temperature dependence, which is why fitting the data using other models fails to reproduce the observed behavior. By isolating the $\xi_{\text{BKT}}(T)$ dependence (Fig. 3(c)) from the T_1^{-1} data we show that the enhancement in $T_1^{-1}(T)$, visible below 150 K, indeed originates from 2D short-range chiral state [17] detected by linewidth $\Delta f(T)$.

BKT correlations have so far been reported in a handful of cases: for $S = 1/2$ systems, in square [32–34] and triangular [3] lattices, and for $S = 1$ in a honeycomb [35] lattice. In each case, correlations were confined to a narrow temperature range, in contrast to CCSF. Surprisingly, despite numerous studies of kagome systems, BKT correlations were not reported to date. To the best of our knowledge, similar behavior was observed only in one other system - the Fe jarosite [36, 37], where the spin of $S = 5/2$ is rather in the classical limit. Interestingly, in that system as well, NS found unconventional XY chiral order [38] above T_N , just like in CCSF. The lack of reports of BKT physics in kagome systems naturally imposes a question on the possible cause. Anisotropy which forces the spins into the kagome plane clearly plays an important role: in Fe-jarosite, DM interaction and/or single-ion anisotropy [36], and in CCSF, a strong DM interaction $d_z = -0.29J$. This is also the reason why in CCSF BKT correlations are visible in zero magnetic field, and in such a wide temperature range [39, 40]. Large DM interaction is also present ($0.18J$) in the “pinwheel” compound RCSF, with a different sign, which has been shown to play an important role [11]: the sign of the DM interaction is connected to the inherited chirality of the triangular lattice and $d_z > 0$ opens a gap that prevents the onset of order. This is why BKT correlations are not observed in the (gapped) “pinwheel” compound RCSF. However, this also indicates that there is a BKT-onset point between RCSF and CCSF that can be reached by doping. A magnetic quantum critical point [9] has been found at $x = 0.53$ in $(\text{Rb}_{1-x}\text{Cs}_x)_2\text{Cu}_3\text{SnF}_{12}$, but there are no reports on underlying excitations of the system. The influence of anisotropy on BKT physics has been theoretically studied for several other cases [41–43], but these are not applicable to the present case.

In summary, we found BKT correlations in the $S = 1/2$ kagome compound $\text{Cs}_2\text{Cu}_3\text{SnF}_{12}$ that persist in a broad temperature range. It onsets together with the 2D XY short range chiral order below $T \sim J_1 \approx 150$ K. By analyzing the zero-field nuclear magnetic resonance spectra, we revise the exact spin structure of the long-range or-

der in this compound. Lack of 2D XY correlations in the sister-compound $\text{Rb}_2\text{Cu}_3\text{SnF}_{12}$ with a VBS ground state, and the availability of $(\text{Rb}_{1-x}\text{Cs}_x)_2\text{Cu}_3\text{SnF}_{12}$ compound that continuously tunes between the two behaviors, shows a direct path for future theoretical and experimental studies on the onset of 2D XY correlations in kagome compounds in general.

We acknowledge fruitful discussions with K. Matan, T. Ono and D. Pajić. We acknowledge the help of M. Novak in developing the high-temperature setup. M.S.G. and I.J. acknowledge the support of Unity Through Knowledge Fund (UKF Grant No. 20/15), Croatian Science Foundation (HRZZ) under the Project No. IP-2024-05-4586 and the support of project CeNIKS co-financed by the Croatian Government and the European Union through the European Regional Development Fund - Competitiveness and Cohesion Operational Programme (Grant No. KK.01.1.1.02.0013).

* corresponding author: mgrbic.phy@pmf.hr

† Current address: Center for Entrepreneurship Education, Institute of Science Tokyo, Midori-ku, Yokohama 226-8502, Japan

- [1] J. Wen, S.-L. Yu, S. Li, W. Yu, and J.-X. Li, Experimental identification of quantum spin liquids, *npj Quantum Materials* **4**, 12 (2019).
- [2] C. Broholm, R. J. Cava, S. A. Kivelson, D. G. Nocera, M. R. Norman, and T. Senthil, Quantum spin liquids, *Science* **367**, eaay0668 (2020), <https://www.science.org/doi/pdf/10.1126/science.aay0668>.
- [3] Z. Hu, Z. Ma, Y.-D. Liao, H. Li, C. Ma, Y. Cui, Y. Shang-guan, Z. Huang, Y. Qi, W. Li, Z. Y. Meng, J. Wen, and W. Yu, Evidence of the Berezinskii-Kosterlitz-Thouless phase in a frustrated magnet, *Nature Communications* **11**, 5631 (2020).
- [4] K. Hwang, K. Park, and Y. B. Kim, Influence of Dzyaloshinskii-Moriya interactions on magnetic structure of a spin- $\frac{1}{2}$ deformed kagome lattice antiferromagnet, *Phys. Rev. B* **86**, 214407 (2012).
- [5] D. Chatterjee, P. Puphal, Q. Barthélemy, J. Willwatter, S. Süllow, C. Baines, S. Petit, E. Ressouche, J. Olivier, K. M. Zoch, C. Krellner, M. Parzer, A. Riss, F. Garmroudi, A. Pustogow, P. Mendels, E. Kermarrec, and F. Bert, From spin liquid to magnetic ordering in the anisotropic kagome Y-kapellasite $\text{Y}_3\text{Cu}_9(\text{OH})_{19}\text{Cl}_8$: A single-crystal study, *Phys. Rev. B* **107**, 125156 (2023).
- [6] M. Hering, F. Ferrari, A. Razpopov, I. I. Mazin, R. Valentí, H. O. Jeschke, and J. Reuther, Phase diagram of a distorted kagome antiferromagnet and application to Y-kapellasite, *npj Computational Materials* **8**, 10 (2022).
- [7] J. Wang, M. Spitaler, Y.-S. Su, K. M. Zoch, C. Krellner, P. Puphal, S. E. Brown, and A. Pustogow, Controlled frustration release on the kagome lattice by uniaxial-strain tuning, *Phys. Rev. Lett.* **131**, 256501 (2023).
- [8] T. Ono, K. Morita, M. Yano, H. Tanaka, K. Fujii, H. Uekusa, Y. Narumi, and K. Kindo, Magnetic susceptibilities in a family of $S = \frac{1}{2}$ kagome antiferromagnets, *Physical Review B* **79**, 174407 (2009).
- [9] K. Katayama, N. Kurita, and H. Tanaka, Quantum phase transition between disordered and ordered states in the spin- $\frac{1}{2}$ kagome lattice antiferromagnet $(\text{Rb}_{1-x}\text{Cs}_x)_2\text{Cu}_3\text{SnF}_{12}$, *Physical Review B* **91**, 214429 (2015).
- [10] K. Matan, T. Ono, Y. Fukumoto, T. J. Sato, J. Yamaura, M. Yano, K. Morita, and H. Tanaka, Pinwheel valence-bond solid and triplet excitations in the two-dimensional deformed kagome lattice, *Nature Physics* **6**, 865 (2010).
- [11] M. S. Grbić, S. Krämer, C. Berthier, F. Trouselet, O. Cépas, H. Tanaka, and M. Horvatić, Microscopic properties of the pinwheel kagome compound $\text{Rb}_2\text{Cu}_3\text{SnF}_{12}$, *Physical Review Letters* **110**, 247203 (2013).
- [12] T. Ono, K. Matan, Y. Nambu, T. J. Sato, K. Katayama, S. Hirata, and H. Tanaka, Large negative quantum renormalization of excitation energies in the spin-1/2 kagome lattice antiferromagnet $\text{Cs}_2\text{Cu}_3\text{SnF}_{12}$, *Journal of the Physical Society of Japan* **83**, 043701 (2014).
- [13] O. Cépas, C. M. Fong, P. W. Leung, and C. Lhuillier, Quantum phase transition induced by Dzyaloshinskii-Moriya interactions in the kagome antiferromagnet, *Physical Review B* **78**, 140405 (2008).
- [14] F. Ferrari, S. Niu, J. Hasik, Y. Iqbal, D. Poilblanc, and F. Becca, Static and dynamical signatures of Dzyaloshinskii-Moriya interactions in the Heisenberg model on the kagome lattice, *SciPost Physics* **14**, 139 (2023).
- [15] K. Matan, T. Ono, G. Gitgeatpong, K. de Roos, P. Miao, S. Torii, T. Kamiyama, A. Miyata, A. Matsuo, K. Kindo, S. Takeyama, Y. Nambu, P. Piyawongwatthana, T. J. Sato, and H. Tanaka, Magnetic structure and high-field magnetization of the distorted kagome lattice antiferromagnet $\text{Cs}_2\text{Cu}_3\text{SnF}_{12}$, *Physical Review B* **99**, 224404 (2019).
- [16] M. Saito, R. Takagishi, N. Kurita, M. Watanabe, H. Tanaka, R. Nomura, Y. Fukumoto, K. Ikeuchi, and R. Kajimoto, Structures of magnetic excitations in the spin- $\frac{1}{2}$ kagome-lattice antiferromagnets $\text{Cs}_2\text{Cu}_3\text{SnF}_{12}$ and $\text{Rb}_2\text{Cu}_3\text{SnF}_{12}$, *Physical Review B* **105**, 064424 (2022).
- [17] K. Matan, T. Ono, S. Ohira-Kawamura, K. Nakajima, Y. Nambu, and T. J. Sato, Breakdown of linear spin-wave theory and existence of spinon bound states in the frustrated kagome-lattice antiferromagnet, *Physical Review B* **105**, 134403 (2022).
- [18] S. Kogure, M. Takeda, K. Morita, Y. Fukumoto, M. Saito, and H. Tanaka, A series expansion study for large negative quantum renormalization of magnon spectra in the $S = 1/2$ kagome-lattice Heisenberg antiferromagnet $\text{Cs}_2\text{Cu}_3\text{SnF}_{12}$, *Journal of the Physical Society of Japan* **92**, 113703 (2023).
- [19] M. Corti, F. Borsa, L. L. Miller, and A. Rigamonti, ^{35}Cl nuclear-magnetic-resonance study of magnetic ordering in $\text{Sr}_2\text{CuO}_2\text{Cl}_2$ single crystal, *Journal of Applied Physics* **75**, 7146 (1994).
- [20] P. Sengupta, A. W. Sandvik, and R. R. P. Singh, Specific heat of quasi-two-dimensional antiferromagnetic Heisenberg models with varying interplanar couplings, *Physical Review B* **68**, 094423 (2003).
- [21] W. Schweika, M. Valldor, and P. Lemmens, Approaching the ground state of the kagomé antiferromagnet, *Phys. Rev. Lett.* **98**, 067201 (2007).
- [22] M. Itoh, S. Hirashima, and K. Motoya, $^{63,65}\text{Cu}$ NMR and NQR study of the Cu^{2+} electronic state and the

- spin dynamics in the spin-Peierls compound CuGeO_3 , *Physical Review B* **52**, 3410 (1995).
- [23] K. Essafi, O. Benton, and L. D. C. Jaubert, Generic nearest-neighbor kagome model: XYZ and Dzyaloshinskii-Moriya couplings with comparison to the pyrochlore-lattice case, *Physical Review B* **96**, 205126 (2017), Note that the chirality convention authors use leads to the opposite sign than ours.
- [24] P. C. Hohenberg and B. I. Halperin, Theory of dynamic critical phenomena, *Reviews of Modern Physics* **49**, 435 (1977).
- [25] T. Moriya, Nuclear magnetic relaxation in antiferromagnetics, *Progress of Theoretical Physics* **16**, 23 (1956).
- [26] A. Abragam, *The principles of nuclear magnetism* (Clarendon Press: Oxford University Press, 1961).
- [27] H. Mayaffre, M. Horvatić, C. Berthier, M.-H. Julien, P. Ségransan, L. Lévy, and O. Piovesana, NMR evidence for a “Generalized spin-Peierls transition” in the high-magnetic-field phase of the spin ladder $\text{Cu}_2(\text{C}_5\text{H}_{12}\text{N}_2)_2\text{Cl}_4$, *Physical Review Letters* **85**, 4795 (2000).
- [28] D. Beeman and P. Pincus, Nuclear spin-lattice relaxation in magnetic insulators, *Phys. Rev.* **166**, 359 (1968).
- [29] M. Jeong, H. Mayaffre, C. Berthier, D. Schmidiger, A. Zheludev, and M. Horvatić, Magnetic-order crossover in coupled spin ladders, *Physical Review Letters* **118**, 167206 (2017).
- [30] N. Laflorencie, Sliding phase in randomly stacked 2d superfluids/superconductors, *Europhysics Letters* **99**, 66001 (2012).
- [31] C. Yasuda, S. Todo, K. Hukushima, F. Alet, M. Keller, M. Troyer, and H. Takayama, Néel temperature of quasi-low-dimensional Heisenberg antiferromagnets, *Physical Review Letters* **94**, 217201 (2005).
- [32] B. J. Suh, F. Borsa, L. L. Miller, M. Corti, D. C. Johnston, and D. R. Torgeson, Spin correlations and magnetic field effects in the weakly anisotropic square-lattice antiferromagnet $\text{Sr}_2\text{CuO}_2\text{Cl}_2$, *Physical Review Letters* **75**, 2212 (1995).
- [33] D. Opherden, M. S. J. Tepaske, F. Bärtl, M. Weber, M. M. Turnbull, T. Lancaster, S. J. Blundell, M. Baenitz, J. Wosnitza, C. P. Landee, R. Moessner, D. J. Luitz, and H. Kühne, Field-tunable Berezinskii-Kosterlitz-Thouless correlations in a Heisenberg magnet, *Physical Review Letters* **130**, 086704 (2023).
- [34] K. M. Ranjith, M. Dupont, S. Krämer, S. Capponi, E. Orignac, N. Laflorencie, N. Kurita, H. Tanaka, and M. Horvatić, *Critical BKT dynamics in the archetypal 2D spin system $\text{Ba}_2\text{CuSi}_2\text{O}_6\text{Cl}_2$* (2025), [arXiv:2511.17381 \[cond-mat.str-el\]](https://arxiv.org/abs/2511.17381).
- [35] M. Heinrich, H.-A. Krug von Nidda, A. Loidl, N. Rogado, and R. J. Cava, Potential signature of a Kosterlitz-Thouless transition in $\text{BaNi}_2\text{V}_2\text{O}_8$, *Physical Review Letters* **91**, 137601 (2003).
- [36] K. Matan, D. Grohol, D. G. Nocera, T. Yildirim, A. B. Harris, S. H. Lee, S. E. Nagler, and Y. S. Lee, Spin waves in the frustrated kagomé lattice antiferromagnet $\text{KFe}_3(\text{OH})_6(\text{SO}_4)_2$, *Physical Review Letters* **96**, 247201 (2006).
- [37] M. Nishiyama, S. Maegawa, T. Inami, and Y. Oka, Magnetic ordering and spin dynamics in potassium jarosite: A Heisenberg kagomé lattice antiferromagnet, *Physical Review B* **67**, 224435 (2003).
- [38] D. Grohol, K. Matan, J.-H. Cho, S.-H. Lee, J. W. Lynn, D. G. Nocera, and Y. S. Lee, Spin chirality on a two-dimensional frustrated lattice, *Nature Materials* **4**, 323 (2005).
- [39] M. Herak, A. Grubišić-Čabo, D. Žilić, B. Rakvin, K. Salamon, O. Milat, and H. Berger, Magnetic anisotropy of the spin tetramer system SeCuO_3 studied by torque magnetometry and ESR spectroscopy, *Phys. Rev. B* **89**, 184411 (2014).
- [40] T. Cvitanić, V. Šurića, K. Prša, O. Zaharko, I. Kupčić, P. Babkevich, M. Frontzek, M. Požek, H. Berger, A. Magrez, H. M. Rønnow, M. S. Grbić, and I. Živković, Singlet state formation and its impact on the magnetic structure in the tetramer system SeCuO_3 , *Phys. Rev. B* **98**, 054409 (2018).
- [41] S. K. Kim and J. Zang, $U(1)$ symmetry of the spin-orbit coupled Hubbard model on the kagome lattice, *Physical Review B* **92**, 205106 (2015).
- [42] H. Li, Y. D. Liao, B.-B. Chen, X.-T. Zeng, X.-L. Sheng, Y. Qi, Z. Y. Meng, and W. Li, Kosterlitz-Thouless melting of magnetic order in the triangular quantum Ising material TmMgGaO_4 , *Nature Communications* **11**, 1111 (2020).
- [43] N. Caci, L. Weber, and S. Wessel, Hierarchical single-ion anisotropies in spin-1 Heisenberg antiferromagnets on the honeycomb lattice, *Physical Review B* **104**, 155139 (2021).